Springer

KSME

Journal of Mechanical Science and Technology 31 (7) (2017) 3157~3170
www.springerlink.com/content/1738-494x(Print)/1976-3824(Online)
DOI 10.1007/s12206-017-0605-3

Nonlinear dynamic response of cable-suspended systems under swinging and heaving motion†

Guohua Cao[1,2,*], Naige Wang[1,2], Lei Wang[1,2] and Zhencai Zhu[1,2]

[1]School of Mechatronic Engineering, China University of Mining and Technology, Xuzhou 221116, China
[2]Jiangsu Key Laboratory of Mine Mechanical and Electrical Equipment, China University of Mining and Technology, Xuzhou 221116, China

(Manuscript Received August 19, 2016; Revised February 28, 2017; Accepted March 28, 2017)

Abstract

In order to enhance the fidelity, convenient and flexibility of swinging motion, the structure of incompletely restrained cable-suspended system controlled by two drums was proposed, and the dynamic response of the system under swinging and heaving motion were investigated in this paper. The cables are spatially discretized using the assumed modes method and the system equations of motion are derived by Lagrange equations of the first kind. Based on geometric boundary conditions and linear complementary theory, the differential algebraic equations are transformed to a set of classical difference equations. Nonlinear dynamic behavior occurs under certain range of rotational velocity and frequency. The results show that asynchronous motion of suspension platform is easily caused imbalance for cable tension. Dynamic response of different swing frequencies were obtained via power frequency analysis, which could be used in the selection of the working frequency of the swing motion. The work will contribute to a better understanding of the swing frequency, cable tension and posture with dynamic characteristics of unilateral geometric and kinematic constraints in this system, and it is also useful to investigate the accuracy and reliability of instruments in future.

Keywords: Incompletely restrained cable-suspended system; Lagrange's equations; Nonlinear dynamics behavior; Swinging and heaving motion

1. Introduction

Cable-driven parallel mechanism used to drive end-effector is composed of winches, platform, cable and base platform. In this mechanism, the platform is hung by suspension cables. It will be a wide use on surface or under water work and the hanging goods. Due to the small moving mass, less expensive, low friction and large workspace, cable-driven parallel mechanisms have been used widely in different applications, such as obstacle avoidances [1, 2], mobile cranes [3, 4], elevators [5, 6], vibration isolator [7], service robotics [8] and construction shaft hoisting systems [9], etc.

Motion control topologies of the cable-driven parallel robots are generally divided into two categories: The full constrained cable-driven mechanism [10, 11] and cable suspended mechanism [12-15]. Cable-driven parallel mechanism (n-DOF) should have at least n+1 cables to completely restrain the moving platform [16, 17] shown in Fig. 1(a). The moving platform of full constrained cable-driven mechanism can obtain high velocities and accelerations in reachable workspace by quickly winding up the cables. However, cable suspended

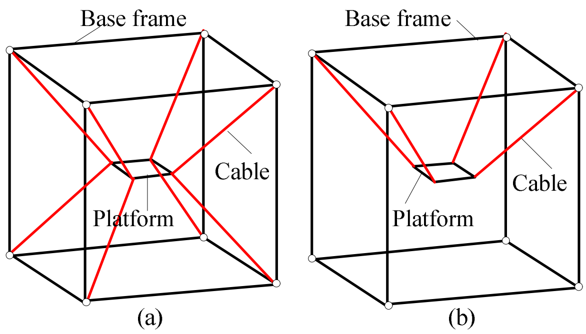

Fig. 1. Full constrained cable-driven mechanism and cable suspended mechanism.

mechanism (Fig. 1(b)) need own gravity to keep its stability [17, 18], which introduces many new challenges in the study of suspended mechanism compared to that of the full constrained cable-driven mechanism. In Refs. [18, 19], they used nonlinear feed forward control laws in the cable length coordinates and proposed optimal tension distribution algorithm to reduce energy usage by the actuators. The spring and damper has been adopted to be installed in the radial direction of the pendulum between the payload and the crane cable for reducing the crane payload sway motion [20]. Dynamic feasible workspace and trajectory planning algorithm of cable-

*Corresponding author. Tel.: +86 13852083536, Fax.: +86 516 83590708
E-mail address: caoguohua@cumt.edu.cn
†Recommended by Associate Editor Eung-Soo Shin

suspended mechanism are also studied in Refs. [21, 22].

Due to the fact that time-varying velocity can result in vibrations of the translating media, the longitudinal vibration during working has immense consequences for performance of the suspended mechanisms. For cable's high slender ratio, some researches are focus on cables simplified as length-variant distributed-parameter components, such as strings, rods and beams. Liu et al. [23] put up with some theoretical tools in researching on longitudinal vibration on FAST. Longitudinal vibration of an elevator system model with homogeneous and inhomogeneous boundary conditions is discussed to study the nature frequency of the elevator [24].

The previous researches focused on the dynamics of one cable with simple boundary conditions. Cable suspended mechanism has many cables with complex boundary conditions. Based on linear boundary condition and a set of independent generalized coordinates, equations of motion applied a spatial discretization and reduction method can be converted to a system of ordinary differential equations to calculate dynamic responses [25, 26]. The reduction method needs independent generalized coordinates to eliminate redundant constraints [27]. A new vector of independent generalized coordinate should be selected and integration restarted when the independent generalized coordinates are changed. When the geometric matching conditions were nonlinear, the reduction method is difficult to select a set of independent generalized coordinates.

As is well-known, in practice the reliability of equipment may be affected by severe shaking. Swing condition is a very complex condition that has become a hidden problem affecting the safety operation of cranes and elevators [28]. Swing and heaving conditions often occur on many transport platforms such as sinking platforms in the mining industry, marine ships when sailing, etc. However, the analysis of swing and heaving condition has not been well-studied in cable suspended mechanisms. Wang et al. [29] have proposed a novel mechanical structure with low power but high load capacity to realize swing environment. They have analyzed its static characteristic based on vector closure conditions. Compared with it, drum driver has been adopted as a new driving system in paper, which has an advantage of swing motion in a large scale. In addition, the tension in the suspension cables should be properly allocated to meet the safety and performance requirements. Hence, it is necessary to evaluate the design by calculating the dynamic responses of the platform and the cables. Asynchronous motion velocities and different frequencies will cause imbalances in cable tension. Nonlinear dynamic behaviors, such as no-smooth phenomenon, will appear at certain range of asynchronous motion velocities and special frequency.

2. Description of IRCSHS

The Incompletely restrained cable-suspended swinging and heaving system (IRCSHS) is designed and shown in Fig. 2, which composed of two drums, sheaves, cables, base frame,

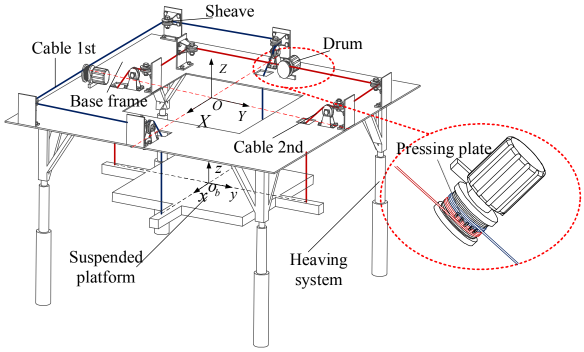

Fig. 2. The model of IRCSHS.

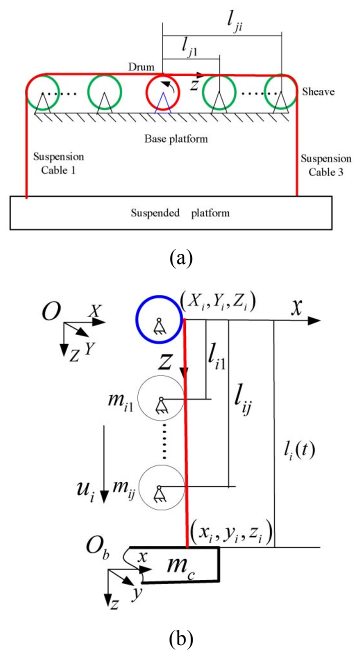

Fig. 3. The model of the ith suspension system model.

suspended platform and heaving system. The cables are winded on the drums respectively, which is shown in Fig. 2. The IRCSHS is equivalent to the suspended platform hang with four suspension cables. The four connected points of the suspension cable are symmetrical distribution around the suspended platform. The cables are fixed on the drums by a pressing plate respectively, and the drums simultaneously control the suspended platform posture by changing the cable length with a periodic motion. The IRCSHS uses suspension cables instead of conventional links, which brings the advantage of the simple structure and low power consumption but at the same time introduces a more complex dynamic behavior.

In order to master the dynamic characteristics of IRCSHS, the substructure to identify the physical parameters of the ith and (i+2)th suspension system is proposed and shown in Fig. 3(a). It assumes that the upper end of each suspension cable is fixed to the drum, while the lower end is attracted to the suspended platform. The longitudinal vibration along the z axial transport motion caused by inevitable elasticity of each cable is depicted in Fig. 3(b). And the Cartesian reference frame $O-XYZ$ is originated at the centroid of the base platform; the Cartesian reference frame O_b-xyz is set at the centroid of suspended platform; the coordinate of the lower ends is (x_i, y_i, z_i) with respect to O_b-xyz; the coordinate of the upper ends is (X_i, Y_i, Z_i) with respect to $O-XYZ$.

The operation of IRCSHS is described as follows: The inputs are the drums displacements and heaving displacement of hydraulic cylinder, and the outputs are the posture of the suspended platform. Each independently controllable drum of the IRCSHS manipulates the suspended platform in space by a spatially arranged cable. When one drum works independently, the swinging motion of suspended platform is formed along a single coordinate axis.

Firstly, equations of motion of IRCSHS are derived from the assumed modes method and Lagrange equations of the first kind, which are a set of Differential algebraic equations (DAEs). The Lagrange's multipliers are adopted to reveal the interaction forces of constrained dynamical systems. Secondly, the resulting spatially discretized equations are converted to the classical Newton-Euler equations of motion applying linear complementary theory [30]. A time discretization scheme [31] is especially suited for the system with unilateral geometric and kinematic constraints. Lastly, the dynamic responses, such as non-smooth phenomenon, are discussed. The suspension cables and the platform components are connected together at the same time, which imposes restrictions on their relative motion, and the operation of large rotations or violent exercise would introduce geometric and tensional nonlinear phenomena. The number of bearing cable would be dynamically changed and determined by its tensioned or loosened condition during this operation. In this paper, the dynamic behaviors of IRCSHS with the nonlinear geometric matching conditions, asynchronous motion velocities and different swing frequencies are systematically investigated.

3. Theoretical model of IRCSHS

3.1 Spatial discretization

The flexible suspension system can be simplified as an axially, moving string with time-varying length and a rigid body mass at its lower end, which is shown in Fig. 3. For the platform mass is much larger than the suspension cable and the length of each suspension cable is relatively short, the lateral vibration of the suspension cables and the influence of the frictional force are ignored. The IRCSHS can be modeled as four cables with varying length and the sheaves can be set as lumped-parameters on cables. The kinetic energy is given by

$$K=\sum_{i=1}^{4}\left(\frac{1}{2}\int_{0}^{l_t}\rho_i\left(\frac{Du_i}{Dt}+v_i\right)^2\mathrm{d}z+\frac{1}{2}\int_{l_{in_t}}^{l_i(t)}\rho_i\left(\frac{Du_i}{Dt}+v_i+v_z\right)^2\mathrm{d}z\right)+\left(\frac{1}{2}m_c\dot{\mathbf{r}}_c^{\mathrm{T}}\cdot\dot{\mathbf{r}}_c+\frac{1}{2}\boldsymbol{\omega}^{\mathrm{T}}\mathbf{I}_c\boldsymbol{\omega}\right) \tag{1}$$

where ρ_i is the mass distribution function of the suspension cable and defined as $\rho_i=\rho+\sum_{j=1}^{n_t}m_{ij}\delta\left(z-l_{ji}\right)$. The angular velocity vector of the suspended platform $\boldsymbol{\omega}$ is determined by the Euler rates with respect to the body-fixed coordinate fame O_b-xyz. The operator D/Dt is given by $D/Dt=\partial/\partial t+v_i\partial/\partial z$.

Similarly, the angular velocity and the linear velocity of the rigid body can be written as

$$\boldsymbol{\omega}=\mathbf{E}\dot{\boldsymbol{\theta}},\dot{\mathbf{r}}_c=\begin{bmatrix}\dot{x} & \dot{y} & \dot{z}\end{bmatrix}^{\mathrm{T}}, \tag{2}$$

where

$$\mathbf{E}=\begin{bmatrix}\cos\beta\cos\gamma & \sin\gamma & 0\\ -\cos\beta\sin\gamma & \cos\gamma & 0\\ \sin\beta & 0 & 1\end{bmatrix},\dot{\boldsymbol{\theta}}=\begin{bmatrix}\dot{\alpha} & \dot{\beta} & \dot{\gamma}\end{bmatrix}^{\mathrm{T}}.$$

The total potential energy can be expressed by

$$\begin{aligned}V=&\sum_{i=1}^{4}\int_{0}^{l_i(t)}\left[T_i(z,t)\varepsilon+\frac{1}{2}EA\varepsilon^2\right]dz\\&-\sum_{i=1}^{4}\int_{l_{ti}}^{l_i(t)}\rho_i g\left(u_i+z\right)dz-m_c gz\end{aligned} \tag{3}$$

where $T_i(z,t)$ is the static tensions in the cables at position z due to the gravitational acceleration g and given as $T_i(z,t)=\rho_i(z)\cdot g\cdot\left(l_i(t)-l_{ti}-z\cdot h(z-l_{ti})\right),(i=1\sim4)$. in which, $h(z-l_{ti})$ is the unit step function. Each cable has the same E and A. The strain ε_i can be approximately expressed as $\varepsilon_i=\partial u_i/\partial z$.

The upper geometric boundary conditions of the suspension cables are obtained as

$$u_i(0,t)=0. \tag{4}$$

The lower geometric matching conditions at the interface between the suspension cable and the suspended platform are described as

$$g_i=l_i(t)+u_i\left(l_i(t),t\right)-\sqrt{\Delta_x(t)^2+\Delta_y(t)^2+\Delta_z(t)^2} \tag{5}$$

where

$$\left[\Delta_x(t),\Delta_y(t),\Delta_z(t)\right]^{\mathrm{T}}=\mathbf{r}_c+\mathbf{R}\left[x_i,y_i,z_i\right]^{\mathrm{T}}-\left[X_i(t),Y_i(t),Z_i(t)\right]^{\mathrm{T}}$$

in which, $\left(X_i(t),\mathrm{Y}_i(t),Z_i(t)\right)$ is the coordinate of the upper ends; the rotation matrix $\mathbf{R}$ can be obtained from basic rotation in term of the roll-pitch-yaw, which can be expressed as

$$\mathbf{R}=\begin{pmatrix}\mathrm{c}\beta\cdot\mathrm{c}\gamma & -\mathrm{c}\beta\cdot\mathrm{s}\gamma & \mathrm{s}\beta\\ \mathrm{c}\alpha\cdot\mathrm{s}\gamma+\mathrm{c}\gamma\cdot\mathrm{s}\alpha\cdot\mathrm{s}\beta & \mathrm{c}\alpha\cdot\mathrm{c}\gamma-\mathrm{s}\alpha\cdot\mathrm{s}\beta\cdot\mathrm{s}\gamma & -\mathrm{c}\beta\cdot\mathrm{s}\alpha\\ \mathrm{s}\alpha\cdot\mathrm{s}\gamma-\mathrm{c}\alpha\cdot\mathrm{c}\gamma\cdot\mathrm{s}\beta & \mathrm{c}\gamma\cdot\mathrm{s}\alpha+\mathrm{c}\alpha\cdot\mathrm{s}\beta\cdot\mathrm{s}\gamma & \mathrm{c}\alpha\cdot\mathrm{c}\beta\end{pmatrix}, \tag{6}$$

where $c(\cdot)$ and $s(\cdot)$ represents shorthand writings for sine and cosine functions, respectively.

Based on the separation of variables method, the longitudinal displacement u_i cab be expressed as

$$u_i(\xi,t)=\sum_{k=1}^{n}U_{i,k}(\xi)q_{i,k}(t) \tag{7}$$

where n represents the number of included modes; a new independent variable $\xi=z/l_i,(z=0\sim l_i)$ is introduced and the time-variant domain [0, l] for z is converted to a fixed domain [0, 1] for ξ. The $U_{i,k}$ should satisfy the homogeneous boundary conditions of Eq. (3), and it can be expressed as

$$U_{i,k}(\xi)=\sqrt{2}\sin(\frac{2k-1}{2}\pi\xi)\,. \tag{8}$$

Substituting the Eqs. (1)-(3) and (5) into the Lagrange equations of the first kind [32]

$$\frac{\partial}{\partial t}\frac{\partial K}{\partial \dot{q}_k}-\frac{\partial K}{\partial q_k}+\frac{\partial V}{\partial q_k}=\sum_{i=1}^{4}\lambda_i\frac{\partial g_i}{\partial q_k} \tag{9}$$

yields the equations of motion

$$\begin{aligned}&\mathbf{M}\ddot{\mathbf{q}}=\mathbf{Q}\left(\mathbf{q},\dot{\mathbf{q}},t\right)+\mathbf{G}_q^{\mathrm{T}}\boldsymbol{\lambda},\\&\mathbf{g}(\mathbf{q},t)=0,\end{aligned} \tag{10}$$

where $\mathbf{q}=(\mathbf{q}_1^{\mathrm{T}},\cdots,\mathbf{q}_4^{\mathrm{T}},\mathbf{r}_c^{\mathrm{T}},\boldsymbol{\theta}^{\mathrm{T}})^{\mathrm{T}}$, ($\mathbf{q}_i=\left[q_{i,1},\cdots,q_{i,n}\right]^{\mathrm{T}}$, i = 1~4) is an array storing the 4n+6 generalized coordinates,; $\mathbf{G}_q^{\mathrm{T}}\boldsymbol{\lambda}$ denotes constraint forces between suspension cables and suspended platform.

And the expressions of $\mathbf{M}$ and $\mathbf{Q}$ could be described as

$$\begin{aligned}&\mathbf{M}=diag(\mathbf{M}^1,\mathbf{M}^2,\mathbf{M}^3,\mathbf{M}^4,\mathbf{M}_c),\\&\mathbf{Q}=\left[\bar{\mathbf{Q}}_1^{\mathrm{T}},\bar{\mathbf{Q}}_2^{\mathrm{T}},\bar{\mathbf{Q}}_3^{\mathrm{T}},\bar{\mathbf{Q}}_4^{\mathrm{T}},\bar{\mathbf{Q}}_c^{\mathrm{T}}\right]^{\mathrm{T}},\end{aligned} \tag{11}$$

in which,

$$\begin{aligned}&\mathbf{M}_c=\begin{bmatrix}m_c\mathbf{I}_3 & \\ & \mathbf{R}^T\mathbf{I}_c\mathbf{R}\end{bmatrix},\\&\bar{\mathbf{Q}}_i=\mathbf{F}^i-\mathbf{C}^i\dot{\mathbf{q}}_i-\mathbf{K}^i\mathbf{q}_i,\quad \bar{\mathbf{Q}}_c=\left[\bar{\mathbf{Q}}_c^1,\bar{\mathbf{Q}}_c^2\right]^{\mathrm{T}},\end{aligned} \tag{12}$$

where $\mathbf{I}_3$ denotes a 3-by-3 identity matrix,

$$\begin{aligned}\mathbf{M}_{ij}^k&=\int_0^1\rho_i l_i\left(t\right)U_iU_jd\xi,\\ \mathbf{C}_{ij}^k&=\int_0^1\rho_i v_iU_iU_jd\xi+v_i\int_0^1\rho_i\left(1-\xi\right)U_i'U_jd\xi\\&\quad-v_i\int_0^1\rho_i\left(1-\xi\right)U_iU_j'd\xi,\\ \mathbf{K}_{ij}^k&=\int_0^1\frac{\rho_i v_i^2\left(1-\xi\right)}{l_i}U_i'U_jd\xi\\&\quad+l_i\int_0^1\rho_i\left[\frac{a_i\left(1-\xi\right)}{l_i}-\frac{v_i^2\left(1-\xi\right)}{l_i^2}+\frac{\xi v_i^2}{l_i^2}\right]U_i'U_jd\xi\\&\quad-\frac{v_i^2}{l_i}\int_0^1\rho_i\left(1-\xi\right)^2U_i'U_j'd\xi+\frac{EA}{l_i}\int_0^1U_i'U_j'd\xi,\\ \mathbf{F}_j^k&=-\int_0^1\left(\rho_i v_i^2+\rho_i\left(a-g\right)l_i\right)U_jd\xi\\&\quad-\int_0^1\left[\rho_i gl_i\left(1-\frac{l_{ti}}{l_i}-\xi\right)h(\xi-\frac{l_{ti}}{l_i})-\rho_i v_i^2\left(1-\xi\right)\right]U_j'd\xi\\&\quad-l_i\int_{\frac{l_{ti}}{l_i}}^1\rho_i a_{zi}\mathrm{d}\xi+l_i\rho_i v_{zi}U_j\left(\frac{l_{ti}}{l_i}\right)\frac{l_{ti}a_i}{l_i^2}\\&\quad+\int_{\frac{l_{ti}}{l_i(t)}}^1\rho_i v_{zi}v\left(1-\xi\right)U_j'\mathrm{d}\xi-\int_0^{\frac{l_{ti}(t)}{l_i(t)}}\rho_i gl_i(t)U_j\mathrm{d}\xi,\\ \bar{\mathbf{Q}}_c^1&=[0\quad 0\quad m_cgz],\\ \bar{\mathbf{Q}}_c^2&=\frac{1}{2}\dot{\boldsymbol{\theta}}^{\mathrm{T}}\left[0,\frac{\partial\mathbf{E}^{\mathrm{T}}}{\partial\beta}\mathbf{I}_c\mathbf{E}+\mathbf{E}^T\mathbf{I}_c\frac{\partial\mathbf{E}}{\partial\beta},\frac{\partial\mathbf{E}^{\mathrm{T}}}{\partial\gamma}\mathbf{I}_c\mathbf{E}+\mathbf{E}^{\mathrm{T}}\mathbf{I}_c\frac{\partial\mathbf{E}}{\partial\gamma}\right]\dot{\boldsymbol{\theta}}\\&\quad-\left[\left(\frac{\partial\mathbf{E}^{\mathrm{T}}}{\partial t}\mathbf{I}_c\mathbf{E}+\mathbf{E}^{\mathrm{T}}\mathbf{I}_c\frac{\partial\mathbf{E}}{\partial t}\right)\dot{\boldsymbol{\theta}}\right]^{\mathrm{T}}.\end{aligned}$$

3.2 Solving method

As described in Eq. (8), the results should meet constrained condition on interface between cables and suspended platform simultaneously. Therefore, the geometric boundary constraints are used to impose design constraints on system responses in a dynamic system, and the equation of motion can be rewritten as

$$\mathbf{M}\ddot{\mathbf{q}}-\mathbf{Q}\left(\mathbf{q},\dot{\mathbf{q}},t\right)-\mathbf{G}_q^{\mathrm{T}}\boldsymbol{\lambda}=\mathbf{0}\,. \tag{13}$$

Taking the time derivative of the constrained condition, the Eq. (4) could be expressed as

$$\dot{\mathbf{g}}=\frac{d\mathbf{g}(q,t)}{dt}=\mathbf{G}_q^{\mathrm{T}}\dot{\mathbf{q}}+\mathbf{G}_t \tag{14}$$

where $\mathbf{G}_t\left(\mathbf{G}_t\in\mathbb{R}^{4\times 1}\right)$ is the time derivative of the constraint equations.

The linear complementarity formulation on velocity level can be written as

$$0\le\dot{\mathbf{g}}\perp\boldsymbol{\Lambda}\ge 0 \tag{15}$$

where, the parameter $\boldsymbol{\Lambda}$ is shown in the Appendix.

Hence, the equation of motion can be converted to differential equation, which is rewritten as

$$\mathbf{M}_M\left(\dot{\mathbf{q}}_E-\dot{\mathbf{q}}_A\right)-\mathbf{Q}_M\mathrm{d}t-\mathbf{G}_{qM}\boldsymbol{\Lambda}=\mathbf{0} \tag{16}$$

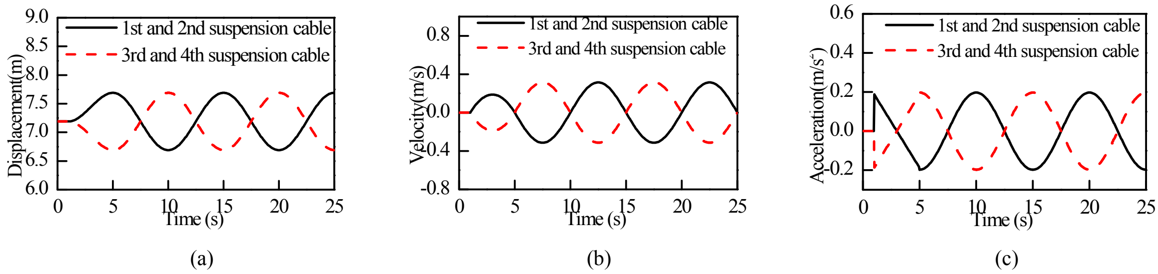

Fig. 4. Swing movement profile.

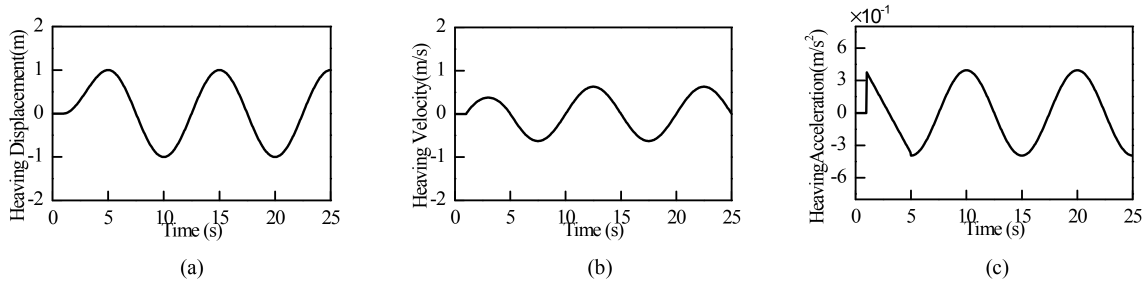

Fig. 5. Heaving movement profile.

in which, $\mathbf{M}_M$, $\mathbf{Q}_M$ and $\mathbf{G}_{qM}$ are the relative matrices of the mass, force vector and the Jacobian matrix of the constraint equations at midpoint of time interval, respectively. $\dot{\mathbf{q}}_A$ and $\dot{\mathbf{q}}_E$ are generalized velocity at two-sided-point of time interval, respectively.

Thus, the generalized velocity $\dot{\mathbf{q}}_E$ of the time of the next step can be expressed as

$$\dot{\mathbf{q}}_E = \mathbf{M}_M^{-1}\mathbf{G}_{qM}\mathbf{\Lambda} + \left(\mathbf{M}_M^{-1}\mathbf{Q}_M \mathrm{d}t + \dot{\mathbf{q}}_A\right). \tag{17}$$

The fixed-step discrete method computes the time of the next calculation step by adding a fixed step size to the current time and the mid-time over the time interval. The preceding process is repeated starting from the initial conditions of the generalized velocity updated by the solution at the end of time intervals. The accuracy and the length of time of the resulting calculation depend on the size of the steps $\mathrm{d}t$ taken by the calculation: The smaller the step size, the more accurate the results are, but the longer time the calculation takes. A more detailed description of derivation process is provided in Appendix.

4. Applications

4.1 Parameters

The parameters for the IRCSHS are listed as follows: $\mathbf{I}_c$ = diag(1.4,1.4,0.8)×10^4 kg·m^2, ρ = 0.9753 kg·m^{-1}, m_c = 1.2 ×10^4 kg, E = 1.2×10^{11} Pa, A = 2.01×10^{-4} m^2. The initial length of each suspension cable is specified at 7.19 m, and the distance between each cable attachment point and the origin of $O_b - xyz$ is 2.07 m.

4.2 Dynamic response of IRCSHS

Swing movement profile about displacement and acceleration curves of the suspension cables are presented in Fig. 4, and heaving movement profile is plotted in Fig. 5. The displacements are sine functions specified at 0.1 Hz, and the jerk is a constant at the first few seconds.

The results of calculation simulation in posture, cable tension and longitudinal vibration are shown in Figs. 6-8, respectively. The posture of the suspended platform, cable tensions and displacements of low ends of suspension cables are presented, indicating that all results are in a reasonable range. From Figs. 6-8, the angles and displacements of the suspended platform represent approximately sinusoidal variation with a sinusoidal excitation. Extra displacements along x axes and y axes are irregular, which mainly comes from the geometrically nonlinear performance of suspension cable and non-linear coupled multidimensional freedom of suspended platform. Thus, it is might difficult to achieve the control objectives simultaneously, because the dynamic behaviors of IRCSHS are affected by many factors, such as the frequency of motion, non-synchronous driving velocities, etc. Under-constrained system is usually challenging to achieve these objectives at the same time, for this reason, the effect of different frequencies and velocities of motion will be analyzed as follows.

4.3 Responses of asynchronous motion velocities

Drum manufacturing error, friction and abrasion wear of groove or irregular cable arrangement can be considered as some source of asynchronous motion velocities of upper ends of cables in real practical problem, and they may play an especially important role in the tension and longitudinal vibration

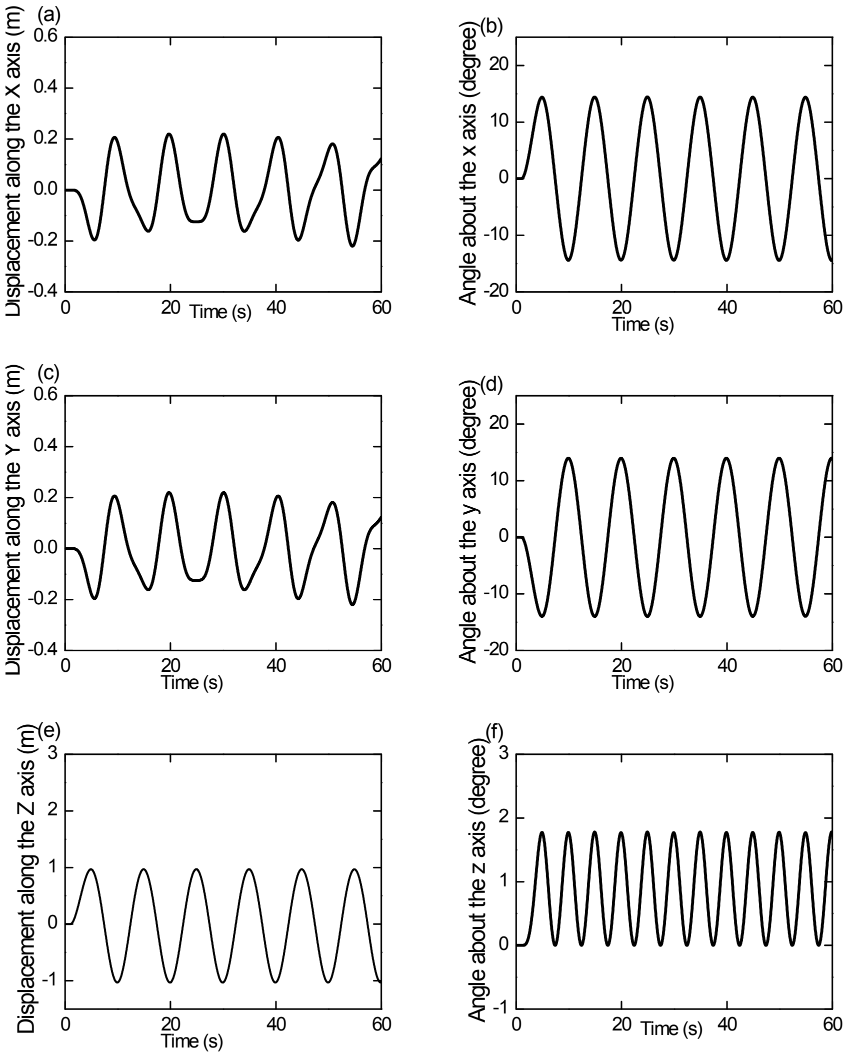

Fig. 6. Posture of the suspended platform.

of short cables. In order to master the dynamic characteristic with asynchronous motion velocities, the motion law of the first three cables is considered to be the same as before, and the velocity of 4th cable on 2nd drum is set as 1.035, 1.05, 1.10 times that of the formers.

Considering that non-smooth phenomena might be caused by kinematic constraints or physical effects, such as cable tension with unilateral properties, geometrical path length of four cables for final solution at the end of a successful step is used to judge the tension cable number for the following step：The governing equations of tension-to-loose cable with free vibration can be removed from the total system; otherwise, the governing equations of loose-to-tension cable can be reintegrated in the total system.

The results of IRCSHS with asynchronous motion velocities about 1.035, 1.05, 1.10 times of other cables are shown in Figs. 8-10. As can be seen from Fig. 10, the tension of 1th cable becomes zero around the time of 10 s, 30 s and 50 s; the 4th cable tension is similar to the former in different time segments, which is in turn significantly effect to abrupt change of displacement and angle about *Z* axis, as it is illustrated in Figs. 9(e) and (f). The asynchronous motion velocities in two drums can lead to no-smooth results which are caused by the unilateral constraint during operation. The parametric study indicates that the time zones of no-smooth phenomenon and the cable tensions increase with the ratio of asynchronous motion velocities. The simulated response of different asynchronous motion velocities as shown in different line styles in Figs. 9(a)-(d) are almost the same.

4.4 Responses of different swing frequencies

With same heaving motion, the cable tension and system stability are heavily influenced by swing excitation frequency, which is one of the critical factors that affect the dynamic performance of IRCSHS. Swing frequencies are varied from low to high, system response of cable tension; longitudinal vibration and posture are shown in Fig. 12. The spectrum am-

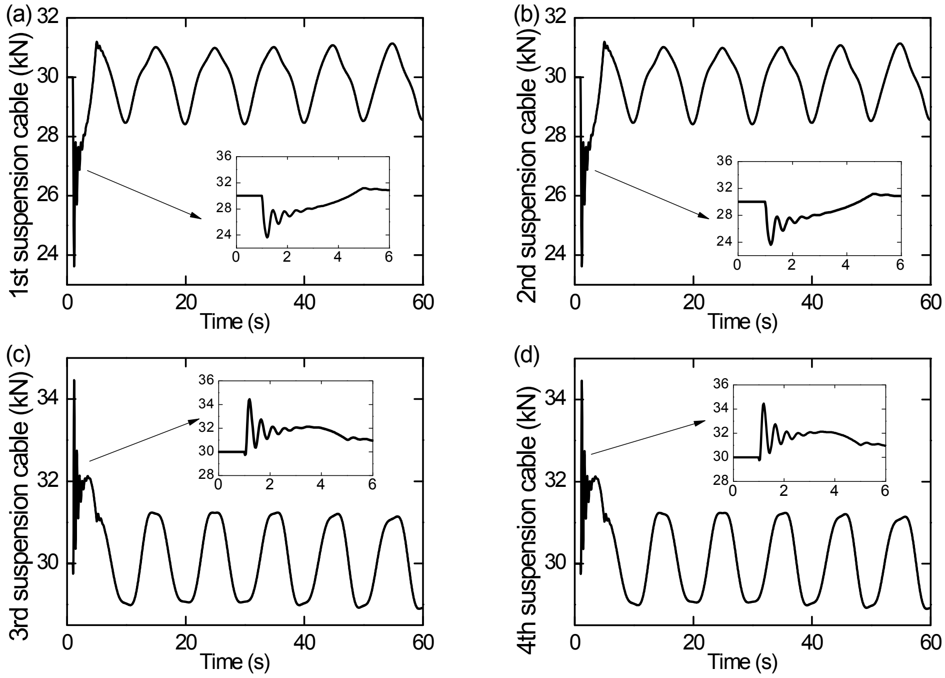

Fig. 7. Cable tensions of low ends of cables.

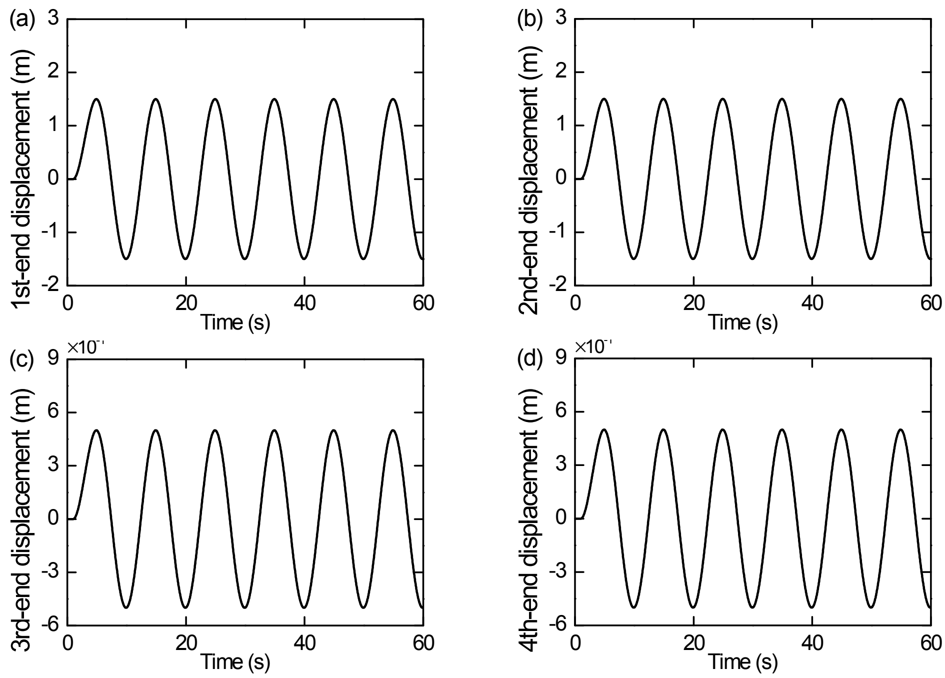

Fig. 8. Longitudinal vibration of low ends of cables.

plitude at a specific swing frequency is a finite number of points. From an overall perspective, swing frequency increases continuously, cable tension and longitudinal vibration also increase gradually in Figs. 12(a) and (b) from low to high. When f_s less than 0.104 Hz, the system response is periodic oscillations with roughly same amplitude. In the parameter region of $0.104\ \text{Hz} \le f_s \le 0.1857\ \text{Hz}$, the width of amplitude area is basically the same. In the interval of $0.1857\ \text{Hz} < f_s \le 0.2053\ \text{Hz}$, the excitations frequency is nearly to the natural frequency of translational degree of freedom in x-axis and y-axis from power spectral analysis of the posture in Fig. 13(a). For this reason, it will bring resonance on translational degree of freedom of x-axis and y-axis. Translational displacement is becoming increasingly and cable will

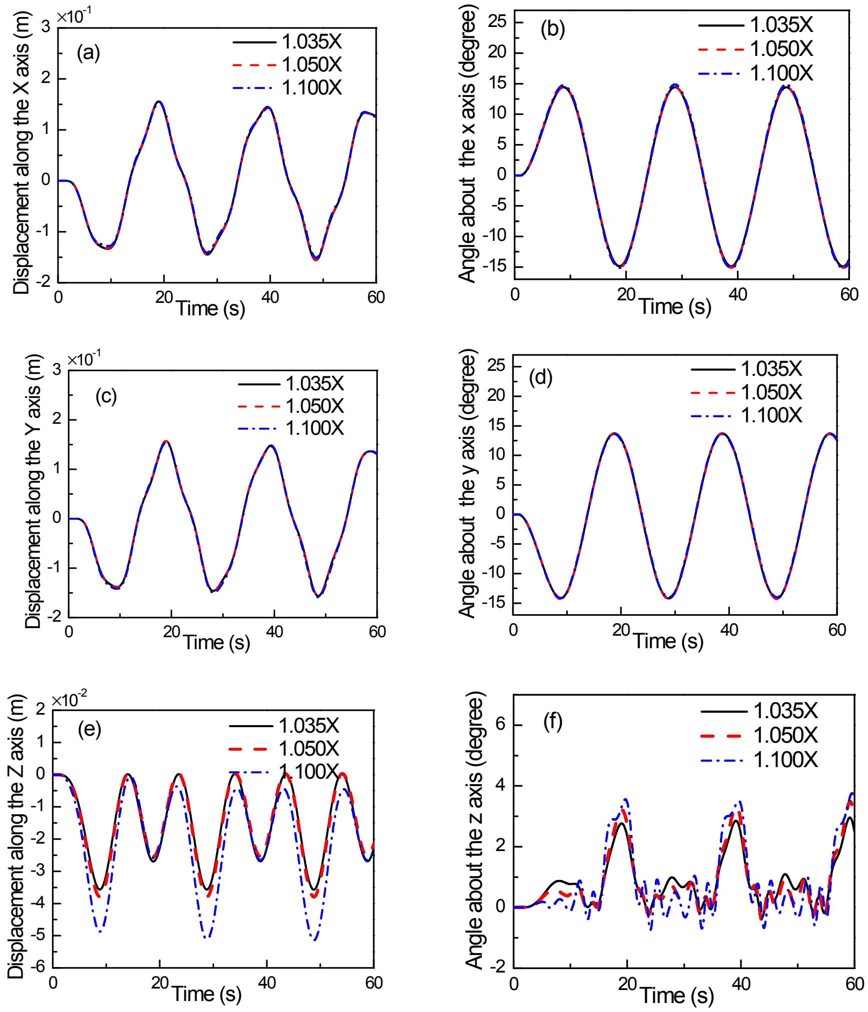

Fig. 9. Posture with different velocities.

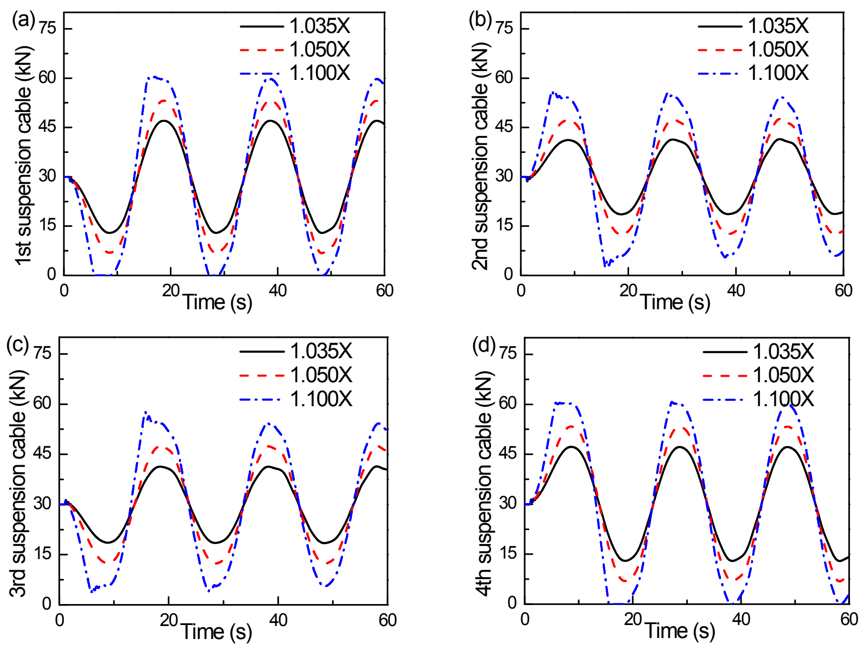

Fig. 10. The tension with different velocities.

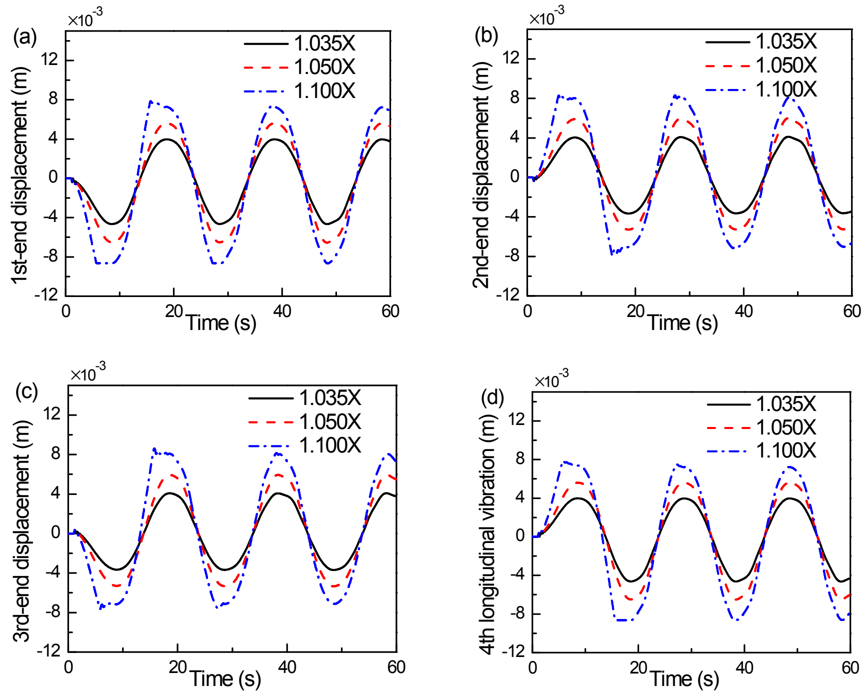

Fig. 11. Longitudinal vibration with different velocities.

sometimes be loose. The results show that the no-smooth phenomenon will happen in the circle of Fig. 12(a). Moreover, as swing frequency changes continuously, the system would soon return to stability when $0.2053\ \text{Hz} < f_s$.

The performance of time characteristics of IRCSHS with $f_s \leq 0.1857$ Hz is similar and shown in Figs. 6-8. System response is a steady period motion at low frequency, and the no-smooth phenomenon does not happen. When the swing frequency equals to 0.223 Hz which is greater than 0.2053 Hz, the time history, phase trajectory and power spectral analysis of the posture on the responses of the IRCSHS are shown in Fig. 13(a). The posture of suspended platform is stable periodic motion on phase trajectory which exhibits a closed curve. It can readily be observed that previous five degree of freedoms of power spectral analysis contains the excitation frequency, and the natural frequency of the vibration system on translational degree of freedom of x-axis and y-axis is 0.186 Hz. However, the response motion of rotational freedom γ is period-doubling-frequency motion. If the swing frequency was 0.191 Hz which is close to the natural frequency, the amplitude of translational degree of freedom gets larger and larger on x-axis and y-axis, which leads to instability of the system.

5. Experimental IRCSHS

To verify dynamic model accuracy compared with the real double-drum driving swing simulation experimental system. In laboratory, a prototype of the IRCSHS is built for experimental tests (Fig. 14). The prototype is a small modeling experiment, which is used to verify the theoretical analysis of the IRCSHS, and the parameters of the prototype model are shown in Table 1.

The implementation of the digital controller and data acquisition which are processed on Pewin32PRO2 and Labview are shown in Fig. 15, which includes a number of enhancements, such as new driven approach and control method. The control hardware includes UMAC, Panasonnic servo motor, HCM365B electronic compass, a host PC and other auxiliary accessories. The control input signal is accomplished by UMPAC before it is converted by driver MADHT and sent to the Panasonnic servo motor for control. The posture signals as signals to the controller after being converted by a HCM365B modular.

Experimental results and theoretical calculation are shown in Fig. 16, from which it can be noticed that simulation results, with consideration of parameter uncertainties and external disturbances, can match experimental results satisfactorily. From power spectrum analysis, frequency components of the swing angle are basically the same, which is useful for testing the efficiency of the proposed analytical approach.

6. Conclusions

The IRCSHS is designed for simulating swing situations and heaving motion in a new way. The nonlinear vibrations of the IRCSHS with flexible suspended cables are investigated under different frequencies and asynchronous motion velocities. The AMM and Lagrange equations of the first kind are combined to establish the equations of motion and a linear

Table 1. Parameters of the prototype model.

Parameter	Description	Value
M	Mass of suspended platform	3.2 kg
A	Cross section area of cable	4.93 mm^2
E	Young's modulus	1.2×10^{11} Pa
g	Gravity acceleration	9.81 m/s^2
ρ	Cable density	0.005 kg/m
l_{s0}	Initial length of suspended portion	0.198 m
l_i	Full length of suspended cable	0.72 m
s	Amplitude displacement	0.024 m
T	Period of motion	10 s

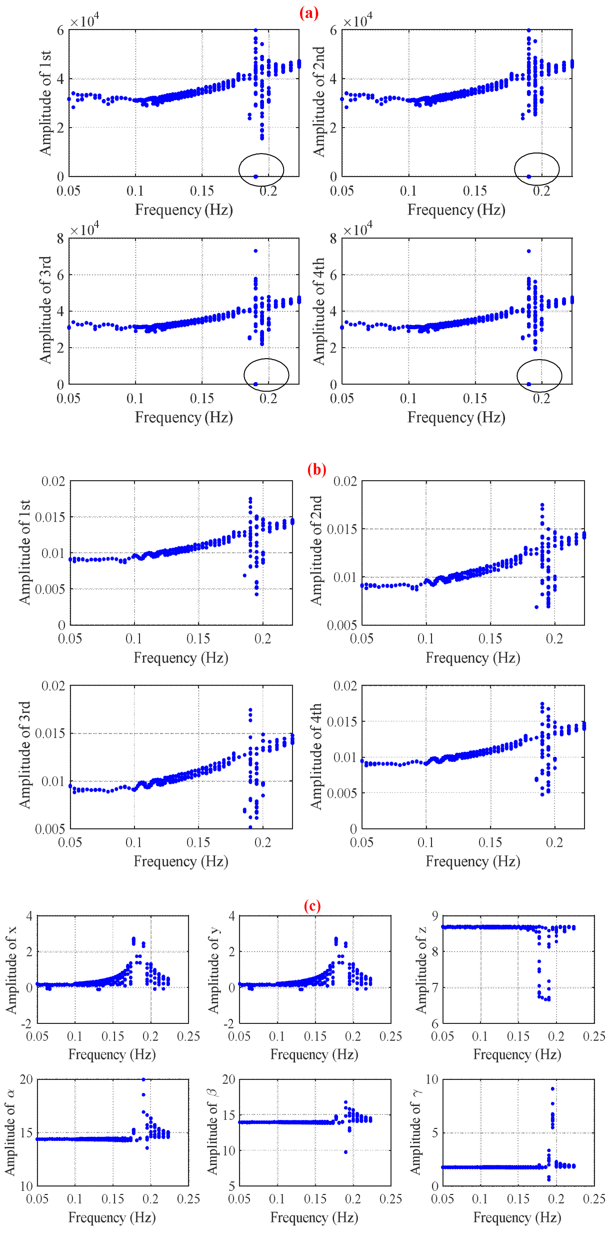

Fig. 12. System response with different swing frequencies.

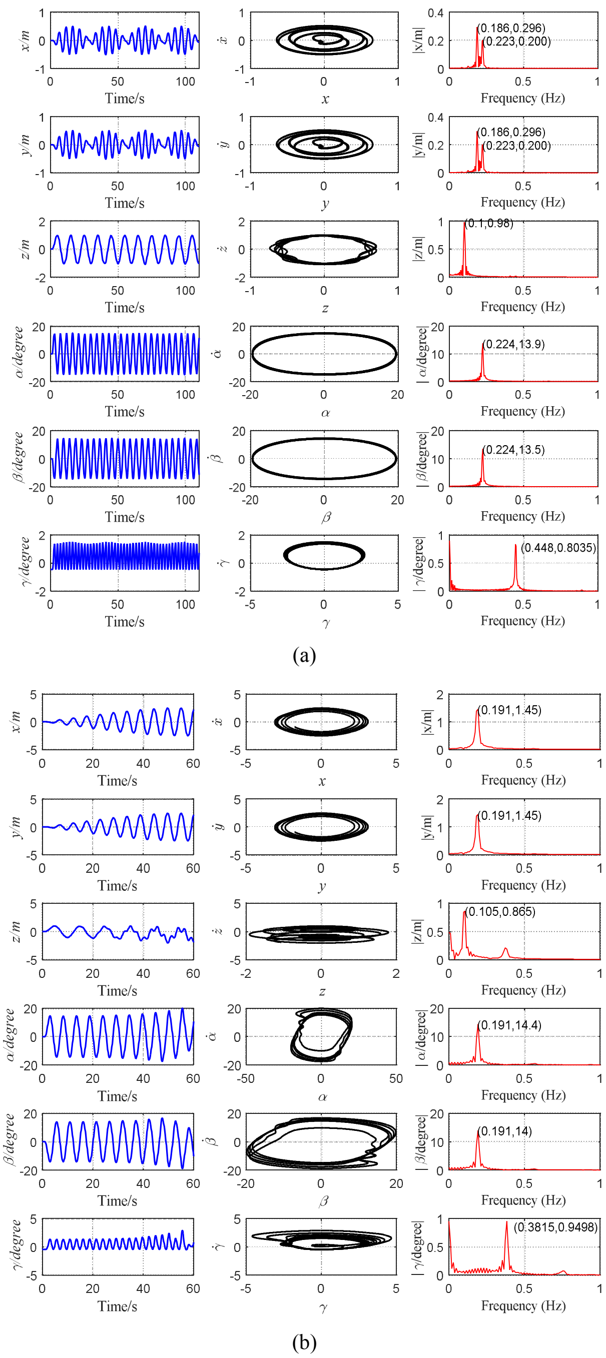

Fig. 13. Phase trajectory and power spectral analysis of the posture with different frequencies: (a) f_s = 0.223 Hz; (b) f_s = 0.191 Hz.

complementarity problem is adopted for solution, which are for working out several challenging problems in the IRCSHS, including the constraint force and the displacement of the suspended platform.

Finally, the effects of various parameters, such as asynchronous motion velocities on two drums and different swing frequencies are discussed. The cable tension difference and asynchronous motion velocities of systems can become larger at specific frequency and lead to no-smooth phenomenon. The

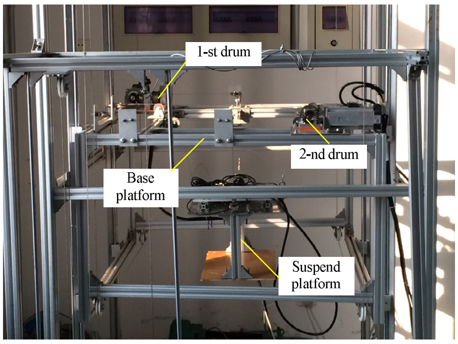

(a)

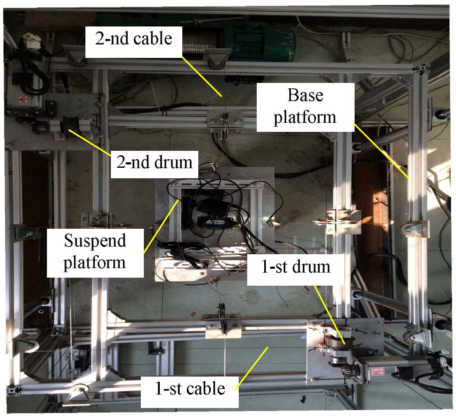

(b)

Fig. 14. Prototype of the IRCSWs2: (a) Front view; (b) top view.

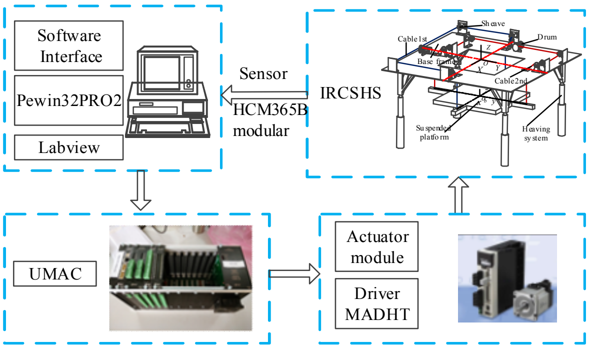

Fig. 15. Block schematic representation of IRCSHS experimental system.

parametric study indicates that the asynchronous motion velocities have a great influence on the cable tension, cable displacement of end point and displacement of the suspended platform about z-axis. The results indicate that the system has both small longitudinal vibration response and position control capacity in low frequency. Based on spectrum amplitude analysis, translation freedom has a low natural frequency; in contrast, the swing excitation frequency has little influence on the stability of swing motion. This work can be guidance of selection for the working frequency of the swing motion. Simulation and experimental results demonstrate that the proposed mechanical structure yields a satisfactory performance.

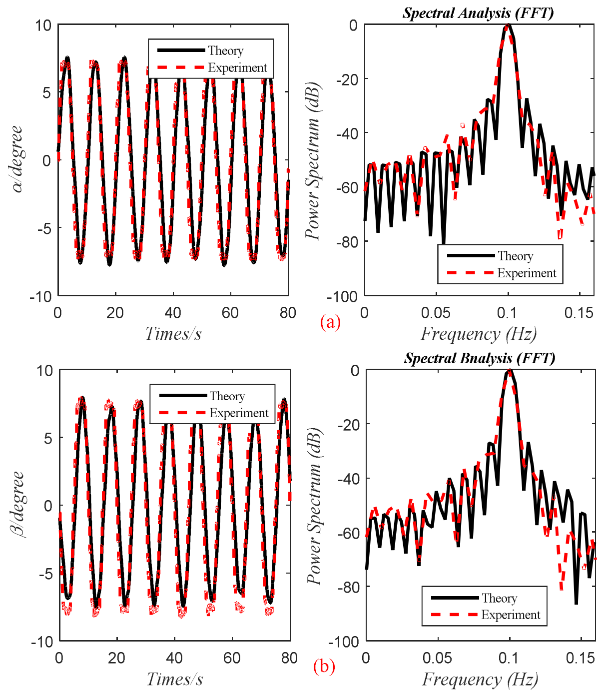

Fig. 16. Experimental result and theoretical calculation.

Acknowledgments

This work is supported by the Fundamental Research Funds for the Central Universities (2017XKQY038) and the Priority Academic Program Development of Jiangsu Higher Education Institutions (PAPD).

Nomenclature

n_t : The number of the sheave of ith suspension cable
m_{ij} : The equivalent mass of sheave of the jth sheave
m_C : The mass of the suspended platform
v_z : The heaving motion velocity
ρ : The unit mass of suspension cable
$\delta(\cdot)$: The Dirac delta function
α : Rotation yaw angle
β : Rotation pitch angle
γ : Rotation roll angle
l_{ti} : The displacement of the n_t th sheave
E : Young's modulus
A : Cross-sectional area
ε_i : Cable strain
l_{ji} : The displacement of the jth sheave in the ith suspension system
$l_i(t)$: The displacement of each suspension cable
$v_i(t)$: Axial translational velocity
$a_i(t)$: Axial translational acceleration
n : The number of included modes

$q_{i,k}$: Generalized coordinates
$U_{i,k}$: The trial function
$\mathbf{g}$: A vector of geometric matching conditions
$\mathbf{M}$: The relative matrices of the mass
$\mathbf{Q}$: Force vector
$\mathbf{G}_q$: The Jacobian matrix of the constraint equations
$\boldsymbol{\lambda}$: Lagrangian multiplier
$\mathbf{I}_c$: The inertia tensor matrix of the suspended platform
$\dot{\mathbf{r}}_c$: The linear displacement vectors
$\boldsymbol{\omega}$: The angular displacement vectors

References

[1] J. Moon and J. V. R. Prasad, Minimum-time approach to obstacle avoidance constrained by envelope protection for autonomous UAVs, *Mechatronics*, 21 (5) (2011) 861-875.

[2] G. S. Chyan and S. G. Ponnambalam, Obstacle avoidance control of redundant robots using variants of particle swarm optimization, *Robotics and Computer-Integrated Manufacturing*, 28 (2) (2012) 147-153.

[3] J. Klosinski, Swing-free stop control of the slewing motion of a mobile crane, *Control Engineering Practice*, 13 (4) (2005) 451-460.

[4] M. Heikkila and M. Linjama, Displacement control of a mobile crane using a digital hydraulic power management system, *Mechatronics*, 23 (4) (2013) 452-461.

[5] H. Taplak, S. Erkaya, S. Yildirim and I. Uzmay, The use of neural network predictors for analyzing the elevator vibrations, *Arabian Journal Forence and Engineering*, 39 (2) (2014) 1157-1170.

[6] L. Q. Shi, Y. Z. Liu, S. Y. Jin and Z. M. Cao, Numerical simulation of unsteady turbulent flow induced by two-dimensional elevator car and counter weight system, *Journal of Hydrodynamics*, 19 (6) (2007) 720-725.

[7] P. S. Balaji et al., Experimental investigation on the hysteresis behavior of the wire rope isolators, *Journal of Mechanical Science and Technology*, 29 (4) (2015) 1527-1536.

[8] J. P. Merlet, Kinematics of the wire-driven parallel robot MARIONET using linear actuators, *IEEE International Conference on Robotics and Automation 2008*, Pasadena, USA (2008) 3857-3862.

[9] X.-G. Shao, Z.-C. Zhu, Q.-G. Wang, P. C. Y. Chen, B. Zi and G.-H. Cao, Non-smooth dynamical analysis and experimental validation of the cable-suspended parallel manipulator, *Proceedings of the Institution of Mechanical Engineers, Part C: Journal of Mechanical Engineering Science*, 226 (10) (2012) 2456-2466.

[10] A. Trevisani, P. Gallina and R. L. Williams II, Cable-direct-driven robot (CDDR) with passive SCARA support: Theory and simulation, *Journal of Intelligent and Robotic Systems*, 46 (1) (2006) 73-94.

[11] M. A. Khosravi and H. D. Taghirad, Robust PID control of fully-constrained cable driven parallel robots, *Mechatronics*, 24 (2) (2014) 87-97.

[12] S. Krut, N. Ramdani, M. Gouttefarde, O. Company and F. Pierrot, A parallel cable-driven crane for Scara-motions, *ASME 2008 International Design Engineering Technical Conferences and Computers and Information in Engineering Conference*, American Society of Mechanical Engineers, Brooklyn, USA (2008) 101-108.

[13] K. Kozak, Q. Zhou and J. S. Wang, Static analysis of cable-driven manipulators with non-negligible cable mass, *IEEE Transactions on Robotics*, 22 (3) (2006) 425-433.

[14] M. H. Korayem and M. Bamdad, Dynamic load-carrying capacity of cable-suspended parallel manipulators, *International Journal of Advanced Manufacturing Technology*, 44 (7) (2009) 829-840.

[15] S. W. Hwang et al., Trajectory generation to suppress oscillations in under-constrained cable-driven parallel robots, *Journal of Mechanical Science and Technology*, 30 (12) (2016) 5689-5697.

[16] A. Trevisani, Underconstrained planar cable-direct-driven robots: A trajectory planning method ensuring positive and bounded cable tensions, *Mechatronics*, 20 (1) (2010) 113-127.

[17] M. Carricato and J. P. Merlet, Stability analysis of under-constrained cable-driven parallel robots, *IEEE Transactions on Robotics*, 29 (6) (2013) 288-296.

[18] M. Carricato, Inverse geometrico-static problem of underconstrained cable-driven parallel robots with three cables, *Journal of Mechanisms and Robotics*, 5 (3) (2013) 1885-1886.

[19] S. Q. Fang, D. Franitza, M. Torlo, F. Bekes and M. Hiller, Motion control of a tendon-based parallel manipulator using optimal tension distribution, *IEEE/ASME Transactions on Mechatronics*, 9 (3) (2004) 561-568.

[20] L. D. Viet, Crane sway reduction using Coriolis force produced by radial spring and damper, *Journal of Mechanical Science and Technology*, 29 (3) (2015) 973-979.

[21] E. Stump and V. Kumar, Workspaces of cable-actuated parallel manipulators, *Journal of Mechanical Design*, 128 (1) (2006) 159-167.

[22] C. B. Pham, S. H. Yeo, G. L. Yang, M. S. Kurbanhusen and I. M. Chen, Force-closure workspace analysis of cable-driven parallel mechanisms, *Mechanism and Machine Theory*, 41 (1) (2006) 53-69.

[23] Z. H. Liu, X. Q. Tang, Z. F. Shao, L. P. Wang and L. W. Tang, Research on longitudinal vibration characteristic of the six-cable-driven parallel manipulator in FAST, *Advances in Mechanical Engineering*, 5 (5) (2013) 547416-547416.

[24] R. M. Chi and H. T. Shu, Longitudinal vibration of a hoist rope coupled with the vertical vibration of an elevator car, *Journal of Sound and Vibration*, 148 (1) (1991) 154-159.

[25] H. Ren and W. D. Zhu, An accurate spatial discretization and substructure method with application to moving elevator cable-car systems-part II: Application, *Journal of Vibration and Acoustics*, 135 (5) (2013) 051037.

[26] W. D. Zhu and H. Ren, An accurate spatial discretization

and substructure method with application to moving elevator cable-car systems-part I: Methodology, *Journal of Vibration and Acoustics*, 135 (5) (2013) 051036.

[27] T. W. Park and E. J. Haug, A hybrid numerical integration method for machine dynamic simulation, *Journal of Mechanical Design*, 108 (2) (1986) 211-216.

[28] P. Williams, Dynamic multibody modeling for tethered space elevators, *58th International Astronautical Congress 2007*, *International Astronautical Federation*, Hyderabad, India (2007) 7372-7392.

[29] N. Wang, G. Cao, Z. Zhu and Y. Wang, Design and trajectory analysis of incompletely restrained cable-suspension swing system driven by two cables, *International Journal of Advanced Robotic Systems*, 12 (1) (2015) 1-13.

[30] P. Flores, R. Leine and C. Glocker, Modeling and analysis of planar rigid multibody systems with translational clearance joints based on the non-smooth dynamics approach, *Multibody System Dynamics*, 23 (2) (2009) 165-190.

[31] S. Ebrahimi and P. Eberhard, A linear complementarity formulation on position level for frictionless impact of planar deformable bodies, *Zamm Journal of Applied Mathematics and Mechanics Zeitschrift Für Angewandte Mathematik Und Mechanik*, 86 (10) (2006) 807-816.

[32] C. Lanczos, *The variational principles of mechanics*, Dover Publications, New York, USA (1986).

[33] C. Gosselin and M. Grenier, On the determination of the force distribution in overconstrained cable-driven parallel mechanisms, *Meccanica*, 46 (1) (2011) 3-15.

Appendix

Introduce the tension of the cables into the equations of governing Eq. (8), the non-smooth dynamics equation can be derived as follow:

$$\mathbf{M}\ddot{\mathbf{q}} - \mathbf{Q} - \mathbf{G}_q\boldsymbol{\lambda} = 0 . \tag{A.1}$$

Multiplied by time step $\mathrm{d}t$, Eq. (A.1) can be expressed as

$$\mathbf{M}\ddot{\mathbf{q}}\mathrm{d}t - \mathbf{Q}\mathrm{d}t - \mathbf{G}_q\boldsymbol{\lambda}\mathrm{d}t = 0 . \tag{A.2}$$

Substituting $\ddot{\mathbf{q}}=\mathrm{d}\dot{\mathbf{q}}/\mathrm{d}t$ and $\Lambda = \boldsymbol{\lambda}\mathrm{d}t$ into Eq. (A.2), and it can obtain

$$\mathbf{M}\frac{\mathrm{d}\dot{\mathbf{q}}}{\mathrm{d}t}\mathrm{d}t - \mathbf{Q}\mathrm{d}t - \mathbf{G}_q\Lambda = 0 . \tag{A.3}$$

Hence,

$$\mathbf{M}\mathrm{d}\dot{\mathbf{q}} - \mathbf{Q}\mathrm{d}t - \mathbf{G}_q\Lambda = 0 . \tag{A.4}$$

Take the total derivative of the constrained condition:

$$\dot{\mathbf{g}} = \frac{\mathrm{d}\mathbf{g}(q,t)}{\mathrm{d}t} = \mathbf{G}_q\dot{q} + \mathbf{G}_t . \tag{A.5}$$

Take the generalized coordinates derivative and the time derivative of the constrained condition in Eq. (4):

$$\mathbf{G}_{q,ij} = \frac{\partial g_i}{\partial q_j} = \frac{\partial}{\partial q_j}\left(\sum_{i=1}^{n} U_i(\xi)q_i(t)\right) - \frac{\partial}{\partial q_j}\sqrt{\Delta_x(t)^2 + \Delta_y(t)^2 + \Delta_z(t)^2} \tag{A.6}$$

$$\mathbf{G}_{t,i} = \frac{\partial g_i}{\partial t} = v_i(t) - \frac{\partial}{\partial t}\sqrt{\Delta_x(t)^2 + \Delta_y(t)^2 + \Delta_z(t)^2} . \tag{A.7}$$

So the linear complementarity formulation the equation on velocity level can be written as

$$0 \le \dot{\mathbf{g}} \perp \boldsymbol{\Lambda} \ge 0 . \tag{A.8}$$

At time $t_M = t_A + \mathrm{d}t/2$, the displacement of state vector is

$$\mathbf{q}_M = \mathbf{q}_A + \dot{\mathbf{q}}_A\mathrm{d}t/2 . \tag{A.9}$$

The differential equation of the system can be written as follow:

$$\mathbf{M}_M\left(\dot{\mathbf{q}}_E - \dot{\mathbf{q}}_A\right) - \mathbf{Q}_M\mathrm{d}t - \mathbf{G}_{qM}\boldsymbol{\lambda}\mathrm{d}t = 0 . \tag{A.10}$$

At the time t_A and t_E

$$\dot{\mathbf{g}}_A = \mathbf{G}_{qM}^T\dot{\mathbf{q}}_A + \mathbf{G}_{tM} \tag{A.11}$$

$$\dot{\mathbf{g}}_E = \mathbf{G}_{qM}^T\dot{\mathbf{q}}_E + \mathbf{G}_{tM} \tag{A.12}$$

$$\dot{\mathbf{q}}_A - \dot{\mathbf{q}}_E = \mathbf{G}_{qM}^{\mathrm{T}}\left(\dot{\mathbf{g}}_E - \dot{\mathbf{g}}_A\right) \tag{A.13}$$

$$\dot{\mathbf{g}}_E = (\mathbf{G}^T_{qM}\mathbf{M}^{-1}_M\mathbf{G}_{qM})\boldsymbol{\Lambda} + (\mathbf{G}^{\mathrm{T}}_{qM}\mathbf{M}^{-1}_M\mathbf{Q}_M\mathrm{d}t + \dot{\mathbf{g}}_A) \tag{A.14}$$

$$\dot{\mathbf{q}}_E = \mathbf{M}_M^{-1}\mathbf{G}_{qM}\boldsymbol{\Lambda} + \mathbf{M}_M^{-1}\mathbf{Q}_M\mathrm{d}t + \dot{\mathbf{q}}_A . \tag{A.15}$$

Guohua Cao received his Ph.D. degree in Mechanical Engineering from China University of Mining and Technology, China, in 2009. Now he is a Professor of CUMT. His research interests include engineering mechanical kinetics, virtual simulation on multi-cable robot and reliability for mechanical system.

Naige Wang is a Ph.D. candidate in Mechanical Engineering from China University of Mining and Technology, China. His research interests include non-linear dynamics of cable robots and vibration control of parallel suspension system.

Lei Wang received his B.S. degree in Mechanical Engineering from China University of Mining and Technology, China, in 2015. Now he is a Ph.D. candidate in CUMT. His research interests include dynamics of the hoisting system and control of the parallel suspension system.

Zhencai Zhu received his Ph.D. degree in China University of Mining & Technology, Xuzhou, China, in 2000. Now he is the Executive President of the Research Academy of CUMT.